Electronic structure of $Cu_{1-x}Ni_xRh_2S_4$ and $CuRh_2Se_4$: Band-structure calculations, x-ray photoemission, and fluorescence measurements

G. L. W. Hart* and W. E. Pickett
Department of Physics, University of California, Davis, California 95616-8677

E. Z. Kurmaev
Institute of Metal Physics, Russian Academy of Sciences–Ural Division, 620219 Yekaterinburg GSP-170, Russia

D. Hartmann and M. Neumann
Department of Physics, University of Osnabrück, Osnabrück D-49069, Germany

A. Moewes
Center for Advanced Microstructures and Devices, Louisiana State University, Baton Rouge, Louisiana 70803

D. L. Ederer
Department of Physics, Tulane University, New Orleans, Louisiana 70118

R. Endoh, K. Taniguchi, and S. Nagata
Department of Materials Science and Engineering, Muroran Institute of Technology, Muroran 050-8585, Japan
(Received 17 June 1999)

The electronic structure of spinel-type $Cu_{1-x}Ni_xRh_2S_4$ ($x=0.0$, 0.1, 0.3, 0.5, 1.0) and $CuRh_2Se_4$ compounds has been studied by means of x-ray photoelectron (XPS) and fluorescent spectroscopy. Cu L_3, Ni L_3, S $L_{2,3}$, and Se $M_{2,3}$ x-ray emission spectra (XES) were measured near thresholds at Beamline 8.0 of the Lawrence Berkeley Laboratory's Advanced Light Source. XES measurements of the constituent atoms of these compounds, reduced to the same binding energy scale, are found to be in excellent agreement with XPS valence bands. The calculated XES spectra which include dipole matrix elements show that the partial density of states reproduce experimental spectra quite well. States near the Fermi level (E_F) have strong Rh d and S(Se) p character in all compounds. In $NiRh_2S_4$ the Ni $3d$ states contribute strongly at E_F, whereas in both Cu compounds the Cu $3d$ bands are only ~ 1 eV wide and centered ~ 2.5 eV below E_F, leaving very little $3d$ character at E_F. The density of states at the Fermi level is less in $NiRh_2S_4$ than in $CuRh_2S_4$. This difference may contribute to the observed decrease, as a function of Ni concentration, in the superconducting transition temperature in $Cu_{1-x}Ni_xRh_2S_4$. The density of states of the ordered alloy $Cu_{0.5}Ni_{0.5}Rh_2S_4$ shows behavior that is more ''split-band''-like than ''rigid-band''-like.

I. INTRODUCTION

Spinel compounds exhibit an extensive variety of interesting physical properties and have potential technological applications. There are a variety of $3d$ ion-based oxide spinels, while the S and Se counterparts usually contain $4d$ or $5d$ atoms. Several of the compounds are superconductors ($LiTi_2O_4$, $CuRh_2S_4$, $CuRh_2Se_4$, etc.), there are unusual magnetic insulators (e.g., $LiMn_2O_4$ and Fe_3O_4), and recently, a d-electron-based heavy fermion metal has been discovered (LiV_2O_4).[1] The suprisingly high value of the superconducting critical temperature (11 K) in $LiTi_2O_4$ has never been understood.[2] Another spinel compound, $CuIr_2S_4$, is neither magnetic nor superconducting but displays a rather unusual metal-insulator transition that is not yet understood.[3] The ternary sulfo- and selenospinels $CuRh_2S_4$ and $CuRh_2Se_4$ have been found to be superconducting at $T_c=4.70$ and 3.48 K, respectively.[4–14] They have the typical spinel structure $[Fd\overline{3}m]$ where Cu ions occupy the A tetrahedral sites and Rh ions occupy the B octahedral sites.

This wide range of phenomena in the spinel-structure oxide compounds raises very general questions about the electronic structure of the sulfides and the selenides: are there indications of strong correlations effects, or can their properties be accounted for as Fermi liquids described by conventional band theory? Different models for the valence of Cu in these compounds have been discussed,[5,6] but according to recent photoemission measurements given for CuV_2S_4,[15] $CuIr_2S_4$, $CuIr_2Se_4$,[16] and $Cu_{0.5}Fe_{0.5}Cr_2S_4$,[17] Cu is best characterized as monovalent in spinel compounds. Therefore, one expects that the Rh ion will have a formal mixed valence of $+3.5$ in $CuRh_2S_4$ and $CuRh_2Se_4$, and indeed both are good metals. However, very little of the typical temperature-dependent behavior of ''mixed valence compounds'' is seen in these Rh-based spinels.

The electrical and magnetic properties of $Cu_{1-x}Ni_xRh_2S_4$ have been presented by Matsumoto *et al.*[18] The superconducting transition temperature decreases (4.70 K$\rightarrow$3.7 K $\rightarrow$2.8 K$\rightarrow<$2.0 K) as Cu is replaced by Ni ($x=0.00$, 0.02, 0.05, and 0.10), but the reason for this behavior is unexplained. Hagino *et al.*[4] have presented extensive data on $CuRh_2S_4$ and $CuRh_2Se_4$ (resistivity, susceptibility, magnetization, specific heat, NMR), but their differences do not yet have any microscopic interpretation. Only for $CuRh_2S_4$ have

general (full potential, all electron) band-structure calculations been reported.[19]

In this paper, we present x-ray spectroscopic studies of the valence band electronic structure of these materials. To provide a clear interpretation of this data, we also report first-principles band-structure calculations [linear-augmented-plane-wave method (LAPW)] for $CuRh_2S_4$, $CuRh_2Se_4$, $NiRh_2S_4$, and $Cu_{0.5}Ni_{0.5}Rh_2S_4$ that enable us to address the properties of these spinels. Total and partial densities of states (DOS), plasma energies and transport-related quantities are calculated as well as x-ray emission spectra. The total and partial DOS and calculated x-ray emission spectra are found to compare favorably with the measured x-ray photoelectron spectra (XPS) and x-ray emission spectra (XES) (which probe total and partial DOS, respectively). All spectral measurements are performed using the same samples which were used to study the electrical and magnetic properties of $Cu_{1-x}Ni_xRh_2S_4$ in Ref. 18.

II. EXPERIMENTAL DETAILS

Mixtures of high-purity fine powders of Cu, Ni, Rh, S, and Se with nominal stoichiometry were heated in sealed quartz tubes at 850° C for a period of 10 days. Subsequently, the specimens were reground and sintered in pressed parallelepiped form at 850° C for 48 h. X-ray-diffraction data confirms the spinel phase in these powder specimens. The lattice constants of $Cu_{1-x}Ni_xRh_2S_4$ are 9.79, 9.79, and 9.71 Å for $x=0.0$, 0.1, and 1.0, respectively, and 10.27 Å for $CuRh_2Se_4$.

The XPS measurements were performed with an ESCA spectrometer from Physical Electronics (PHI 5600 ci, with monochromatized Al K_α radiation of a 0.3 eV fullwidth at half maximum). The energy resolution of the analyzer was 1.5% of the pass energy. The estimated energy resolution was less than 0.35 eV for the XPS measurements on the copper and nickel sulfides. The pressure in the vacuum chamber during the measurements was below 5×10^{-9} mbar. Prior to XPS measurements the samples were cleaved in ultrahigh vacuum. All the investigations have been performed at room temperature on the freshly cleaved surface. The XPS spectra were calibrated using an Au foil to obtain photoelectrons from the Au $4f_{7/2}$ subshell. The binding energy for Au $4f_{7/2}$ electrons is 84.0 eV.

X-ray fluorescence spectra were measured at Beamline 8.0 of the Advanced Light Source at Lawrence Berkeley Laboratory. The undulator beam line is equipped with a spherical grating monochromator,[20] and an experimental resolving power of $E/\Delta E=300$ was used. The fluorescence end station consists of a Rowland circle grating spectrometer. The Ni L_3 and Cu L_3 XES were measured with an experimental resolution of approximately 0.5–0.6 eV and S $L_{2,3}$ and Se $M_{2,3}$ with resolution of 0.3–0.4 eV. The incident angle of the p-polarized monochromatic beam on the sample was about 15°. The Cu L_3 and Ni L_3 XES were measured just above the L_3 threshold but below the L_2 threshold which prevented overlap of the metal L_3 and metal L_2 spectra.

III. METHOD OF CALCULATION

The band-structure calculations were done with the full potential LAPW code WIEN97.[21] The sphere radii were chosen as 2.1, 2.2, and 2.0 a.u. for Cu/Ni, Rh, and S/Se, respectively. The plane-wave cutoff was $K_{max}=3.25$ a.u., resulting in slightly more than 1400 basis functions per primitive cell ($\sim$100 basis functions/atom). The local-density approximation (LDA) exchange-correlation potential of Perdew and Wang[22] was used. Because the Fermi level falls on a peak in the DOS for $NiRh_2S_4$, as shown in Fig. 7, the gradient correction to the LDA exchange-correlation potential of Perdew, Burke, and Ernzerhof[23] was used in the DOS calculations shown in Fig. 7. A mesh of 47 k points in the irreducible zone (Blöchl *et al.*'s modified tetrahedron method[24]) was used in achieving self-consistency.

The XES spectra were calculated using Fermi's golden rule and the matrix elements between the core and valence states (following the formalism of Neckel *et al.*[25]). The calculated spectra include broadening for the spectrometer and core and valence lifetimes. The DOS calculations used 47 k points (again, Blöchl's modified tetrahedron method was used). The experimental lattice constants (listed in the previous section) were used in the calculations and the values used for the internal parameter u were taken to be 0.385 for all three stoichiometric compounds ($CuRh_2Se_4$, $CuRh_2S_4$, $NiRh_2S_4$) as well as for $Cu_{0.5}Ni_{0.5}Rh_2S_4$. Experimental data for the internal parameter was not available, so the values were taken to be 0.385 (rather than the ''ideal'' position of 3/8) by analogy to the related $CuIr_2S_4$ and $CuIr_2Se_4$ spinel compounds for which the u parameter has been measured.[3]

IV. DISCUSSION OF SPECTROSCOPIC DATA

A. $CuRh_2S_4$ and $NiRh_2S_4$

The calculated total and partial DOS of $CuRh_2S_4$ and $NiRh_2S_4$, shown in Figs. 1 and 2, respectively, reveal many common features. The valence bands extend from E_F (taken as the zero of energy) to approximately -7 eV and the Fermi level lies near the top of a Rh d–chalcogen p complex of bands that lie below a gap centered 0.5–1.0 eV above the Fermi level. The gap between the valence band and conduction band is found to be about 0.5–0.7 eV wide. The sulfur states in $CuRh_2S_4$ and $NiRh_2S_4$ show similar DOS, S $3s$ atomic like states in the region $-12.7\sim-14.7$ eV and band-like S $3p$ states which are mixed with Rh $4d$ and Cu/Ni $3d$ states in a wide energy region. Cu/Ni $3d$ states are found to be much narrower than Rh $4d$ states which are less localized and form several large peaks in the DOS near the bottom and the top of the valence band. Our results for $CuRh_2S_4$ are similar to those of Ref. 19 except for the distribution of Cu $3d$ DOS.[26] As seen in Fig. 1, Cu $3d$ states lie within the region of S $3p$ states but are weakly hybridized, forming a 1 eV wide peak centered around -2.5 eV. The S d character is quite small and probably reflects tails of the neighboring atoms more than atomic $3d$ character.

The total DOS at the Fermi level $[N(E_F)]$ increases from $NiRh_2S_4$ (8.18 states/eV/cell) to $CuRh_2S_4$ (9.89 states/eV/cell) which has the same trend as electronic specific-heat coefficients measured in Refs. 4 and 27. For the intermediate compound $Cu_{0.5}Ni_{0.5}Rh_2S_4$, $N(E_F)$ is 8.43 states/eV/cell, much nearer that of $NiRh_2S_4$. In $CuRh_2S_4$ the Cu $3d$ partial DOS is very small at the Fermi level whereas Rh $4d$ and S $3p$ partial DOS are the main contribution to the total. Con-

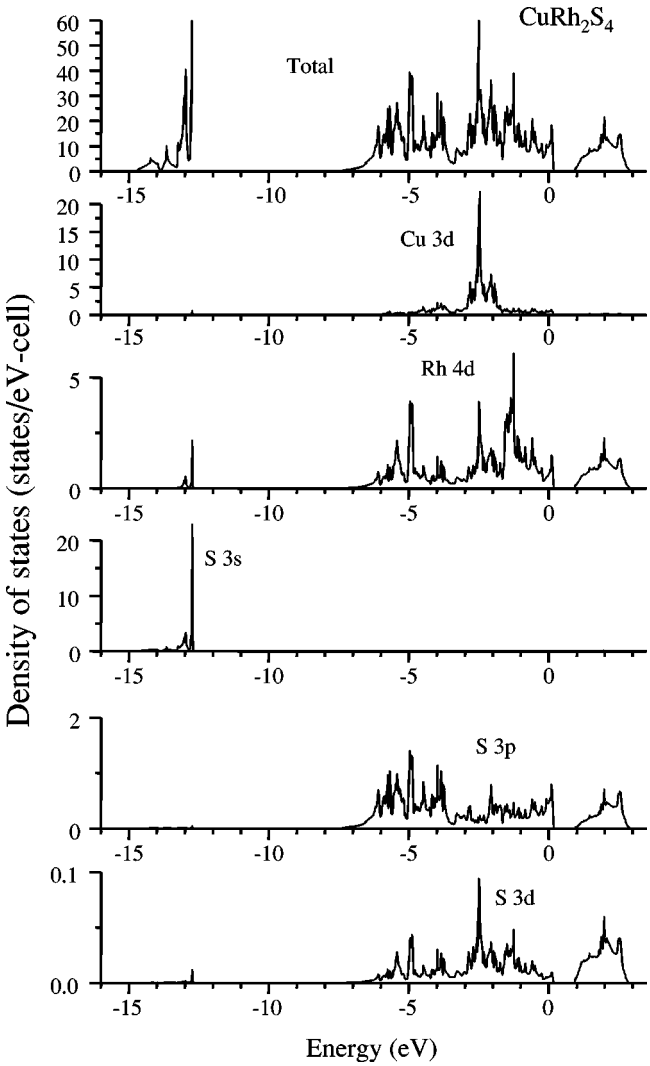

FIG. 1. Calculated total (top panel) and partial DOS in $CuRh_2S_4$. Note the hybridization gap that lies just above the Fermi level (taken as the zero of energy), indicating the Fermi level lies in a bonding region of the electronic structure.

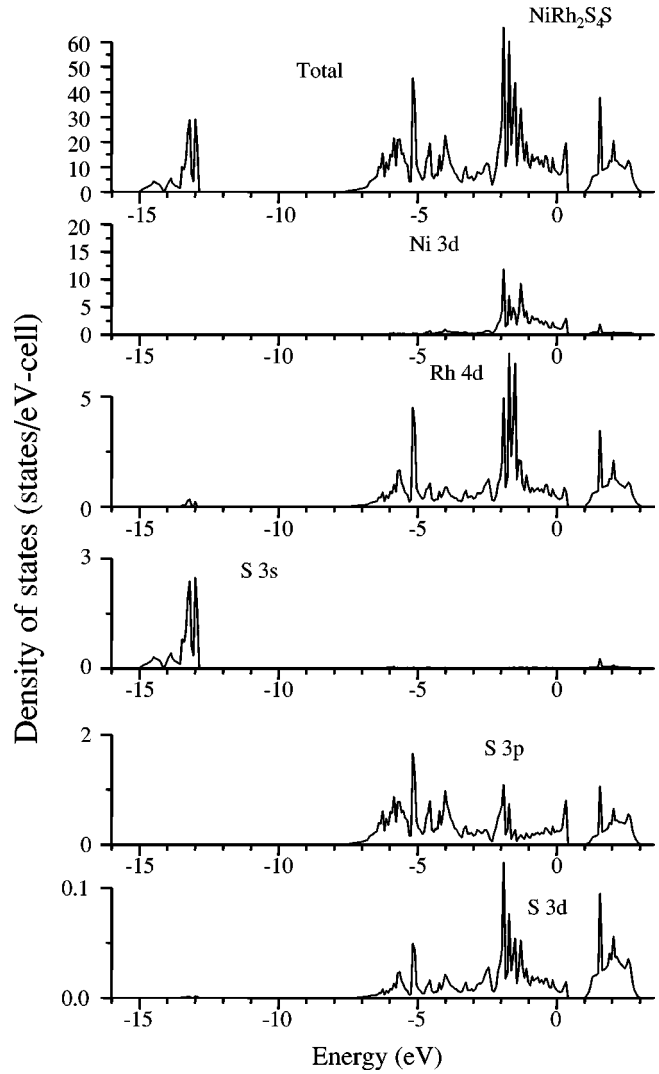

FIG. 2. Calculated total (top panel) and partial DOS as in Fig. 1 but for $NiRh_2S_4$.

sequently, the Cooper pairs in the superconducting state of $CuRh_2S_4$ are formed mainly by the electrons in the hybridized bands derived from Rh $4d$ and S $3p$ states. Several characteristic materials parameters are collected in Table I for easy comparison.

In $NiRh_2S_4$ the situation is quite different. Ni $3d$ states are broader and at lower binding energy than the Cu $3d$ states of $CuRh_2S_4$, and hybridization with S p leads to Ni $3d$ character over a 3 eV wide region that extends above the Fermi level. The result is that the main contribution to the DOS at the Fermi level is from Ni $3d$ states, unlike in $CuRh_2S_4$ where the Cu $3d$ contribution at E_F is very minor.

The experimental Cu L_3 ($3d4s \rightarrow 2p$ transition), Ni L_3 ($3d4s \rightarrow 2p$ transition), and S $L_{2,3}$ ($3s3d \rightarrow 2p$ transition) XES probe Cu $3d4s$, Ni $3d4s$, and S $3s3d$ partial DOS in the valence band and, in the first approximation, can be directly compared with calculated band structures. The comparison of the calculated and measured partial DOS are shown in Figs. 3 and 4, where Cu L_3, Ni L_3, and S $L_{2,3}$ XES are converted to the binding-energy scale using our XPS measurements of the corresponding core levels [$E_{\text{b.e.}}(\text{Cu } 2p) = 932.39$ eV, $E_{\text{b.e.}}(\text{Ni } 2p) = 852.98$ eV and $E_{\text{b.e.}}(\text{S } 2p) = 161.57$ eV]. We see that the measured Cu L_3, Ni L_3, and S $L_{2,3}$ XES peaks are very close to Cu $3d$, Ni $3d$, and S $3s$ partial DOS in $CuRh_2S_4$ (Fig. 3) and $NiRh_2S_4$ (Fig. 4). In each case, the peaks in the calculated DOS lie at somewhat lower binding energy: 1 eV for S $3s$ and Cu $3p$, but only a few tenths of eV for Ni $3d$. The difference reflects a self-energy correction that lies beyond our band theoretical methods. In addition, we calculated the emission intensities of Cu/Ni L_3, Rh $N3$ ($4d \rightarrow 4p$ transition)[28] and S $L_{2,3}$ XES in both compounds as described in Sec. III. The calculated spectra are presented in the same figures (Figs. 3 and 4) and show close correspondence with experimental spectra as well as with the corresponding partial DOS. From the close agreement, we conclude that the influence of core holes in the measured XES spectra is minor and experimental spectra can be understood directly from the calculated spectra and partial DOS.

B. $Cu_{1-x}Ni_xRh_2S_4$ ($x = 0$, 0.1, 0.3, 0.5, 1.0)

We measured XPS valence band (VB) spectra for the $Cu_{1-x}Ni_xRh_2S_4$ ($x = 0$, 0.1, 0.3, 0.5, 1.0) system (see Fig. 5)

TABLE I. Transport related quantities and other data.

	$NiRh_2S_4$	$Cu_{0.5}Ni_{0.5}Rh_2S_4$	$CuRh_2S_4$	$CuRh_2Se_4$
a (Å)	9.71	9.75 (assumed)	9.79	10.27
$N(E_F)$ (states/eV cell)	8.18	8.43	9.89	12.05
$N(E_F)$ Hagino *et al.* (Ref. 4)		12.6	13.4	
v_F (10^7 cm/s)	2.49	2.22	1.79	1.75
$\hbar\Omega_p$ (eV)	2.41	2.17	1.89	1.89
T_c (K)	<2.0		4.70	3.483 (Ref. 4)

and found a four-peak structure: (a, c, d, e) for $CuRh_2S_4$ and (a, b, d, e) for $NiRh_2S_4$, each of which is very close to the corresponding calculated total DOS (Figs. 1 and 2). Based on our calculations, we can conclude that the a peak at 1 eV binding energy is formed by Rh $4d$–S $3p$ states for $CuRh_2S_4$ and Ni $3d$–Rh $4d$–S $3p$ states for $NiRh_2S_4$. The next peak (b for $NiRh_2S_4$ at 2 eV binding energy and c for $CuRh_2S_4$ at 3 eV binding energy) can be attributed mainly to Ni (respectively Cu) $3d$ states. The d peak (5.5 eV) relates to Rh $4d$–S $3p$ states and the e peak is associated with atomiclike S $3s$ states. In the solid solution $Cu_{1-x}Ni_xRh_2S_4$ the positions of the peaks do not change as the concentration varies, but only the ratio of intensities of b (Ni $3d$) and c (Cu $3d$) peaks vary according to the Cu/Ni concentration.

This behavior suggests that the electronic structure of the solid solution $Cu_{1-x}Ni_xRh_2S_4$ can be deduced by analyzing the endpoints ($x=0.0$ and 1.0), $CuRh_2S_4$ and $NiRh_2S_4$. This conclusion results not from a rigid-band picture (which does not hold) but from the opposite ''split-band'' behavior[29] in which both Cu and Ni retain their own DOS peaks (see Fig. 11) which then vary in strength roughly as the concentration. In Fig. 6 we have compared XPS VB measurements with Cu L_3, Ni L_3, and S $L_{2,3}$ XES spectra for $Cu_{0.5}Ni_{0.5}Rh_2S_4$.[30] We see that positions of the peaks in the Ni L_3, Cu L_3, and S $L_{2,3}$ XES spectra correspond exactly to peaks b, c, and e of the XPS VB measurements, which is consistent with our interpretation of the XPS data as indicating a solid solution of $Cu_{1-x}Ni_xRh_2S_4$ if the split-band behavior holds.

In Fig. 7 we have compared the calculated total DOS of $CuRh_2S_4$, $NiRh_2S_4$, and $Cu_{0.5}Ni_{0.5}Rh_2S_4$. With respect to the top of the highest occupied bands, the Fermi energy is highest in the bands of $CuRh_2S_4$ to accommodate the two additional electrons from the Cu atoms. The behavior of the DOS for the three systems shown are quite different, particularly for Cu and Ni ions, in an energy range between the Fermi levels for $NiRh_2S_4$ and for $CuRh_2S_4$, invalidating a rigid-band interpretation of the differences and similarities in these compounds. This is not surprising given the different

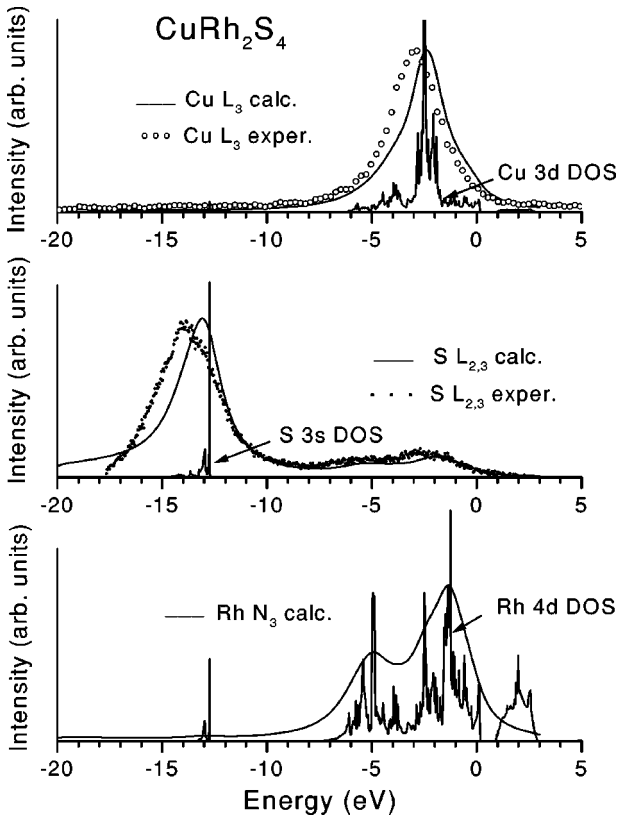

FIG. 3. Comparison of calculated XES and partial DOS with experimental spectra of $CuRh_2S_4$. Calculations used the LAPW method as described in the text.

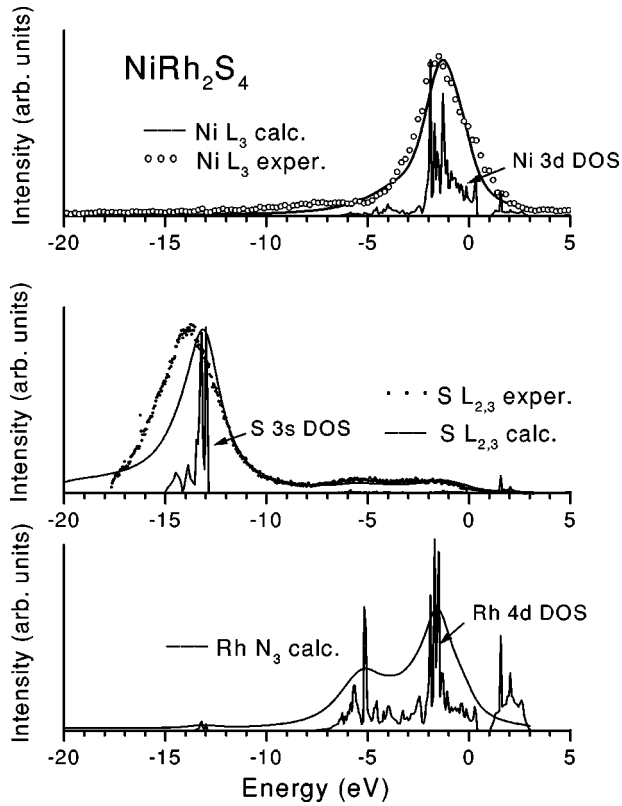

FIG. 4. Comparison of calculated XES and partial DOS with experimental spectra of $NiRh_2S_4$.

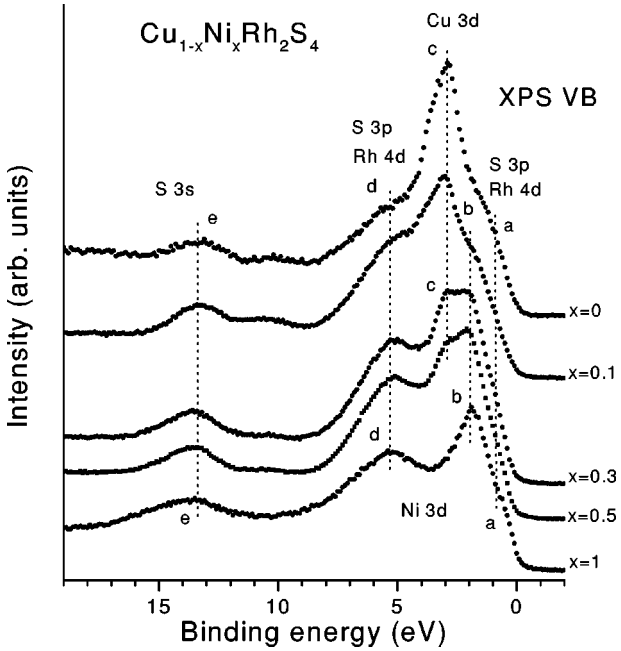

FIG. 5. XPS VB of $Cu_{1-x}Ni_xRh_2S_4$ ($x=0.0$, 0.1, 0.3, 0.5, 1.0). The peaks and shoulders a,b,c,d,e are discussed in the text.

character of the Ni- and Cu-derived states in this energy region. As mentioned above, whereas states at the Fermi level in $NiRh_2S_4$ have a strong Ni 3d character, Cu 3d states lie entirely below the Fermi level in $CuRh_2S_4$. The character of states at the Fermi level in $CuRh_2S_4$ are primarily Rh d-like states hybridized with S 3p states.

According to Ref. 18, the superconducting transition temperature of $Cu_{1-x}Ni_xRh_2S_4$ decreases with increasing Ni concentration from 4.7 K ($x=0.0$) to 3.7 K ($x=0.02$) and then to 2.8 K ($x=0.05$). While we attribute this to a general decrease in DOS at the Fermi level as the Ni concentration is increased (see Sec. V), this trend does not require a simple rigid-band interpretation. In the alloy, the DOS within a few tenths of an eV of E_F probably cannot be described by either the rigid band or split-band models.

C. $CuRh_2Se_4$

Figure 8 shows the calculated total and partial DOS for $CuRh_2Se_4$. While it is similar to that of $CuRh_2S_4$ (Fig. 1), we

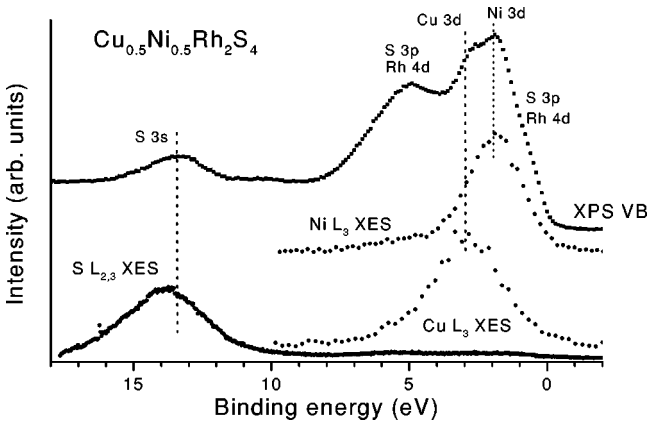

FIG. 6. Comparison of the valence band XPS spectrum (upper set of data) to the Cu L_3, Ni L_3, and S $L_{2,3}$ XES in $Cu_{0.5}Ni_{0.5}Rh_2S_4$. Note the close alignment of XPS and XES peaks.

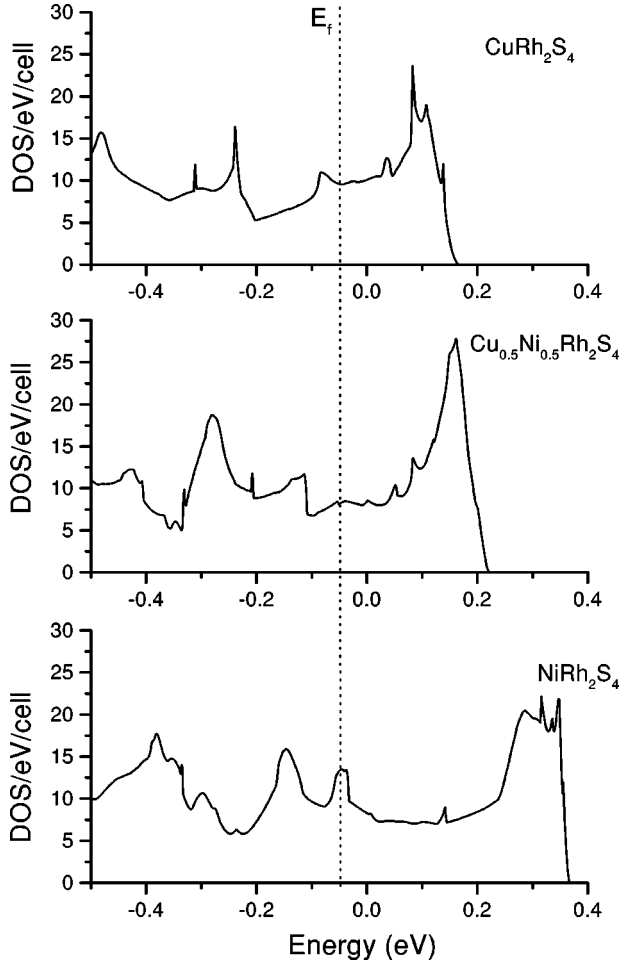

FIG. 7. Calculated total DOS of $NiRh_2S_4$, $Cu_{0.5}Ni_{0.5}Rh_2S_4$, and $CuRh_2S_4$ aligned to the top of the valence band. Note that, despite the general similarities, a rigid-band-interpretation is not applicable.

can point out two differences: (i) the Se 4p DOS is redistributed somewhat compared to S 3p and has a higher contribution in the vicinity of the Fermi level, and (ii) the Se d-like character is even less than that of the d-like character in $CuRh_2S_4$. The total DOS at the Fermi level is 12.05 states/eV cell which is higher than in $CuRh_2S_4$, in qualitative agreement with measurements of electronic specific-heat measurements.[4]

In Fig. 9 the experimental Cu L_3 and Se $M_{2,3}$ ($4s\rightarrow 3p$ transition) XES measurements are compared to the Cu 3d and Se 4s partial DOS and calculated spectra. The agreement of the peak positions between experiment and theory is quite close. Again we note that calculated XES spectra exactly follow the partial DOS, as in the case of $CuRh_2S_4$ and $NiRh_2S_4$ (Figs. 3 and 4). The XPS valence band data is compared with the Cu L_3 and Se $M_{2,3}$ XES spectra of Fig. 10. The location of Cu 3d–Se 4s-derived bands is reproduced well (comparable to that in the sulfide) by the calculations. There are some differences in ratio of the XPS peaks for $CuRh_2Se_4$ and $CuRh_2S_4$: the relative intensity of Cu 3d peak located at around 2.5 eV is less in $CuRh_2Se_4$ than in $CuRh_2S_4$. This may be due to the 2.5 times larger photoionization cross section of Se 4p states as compared to that of S 3p states.[31]

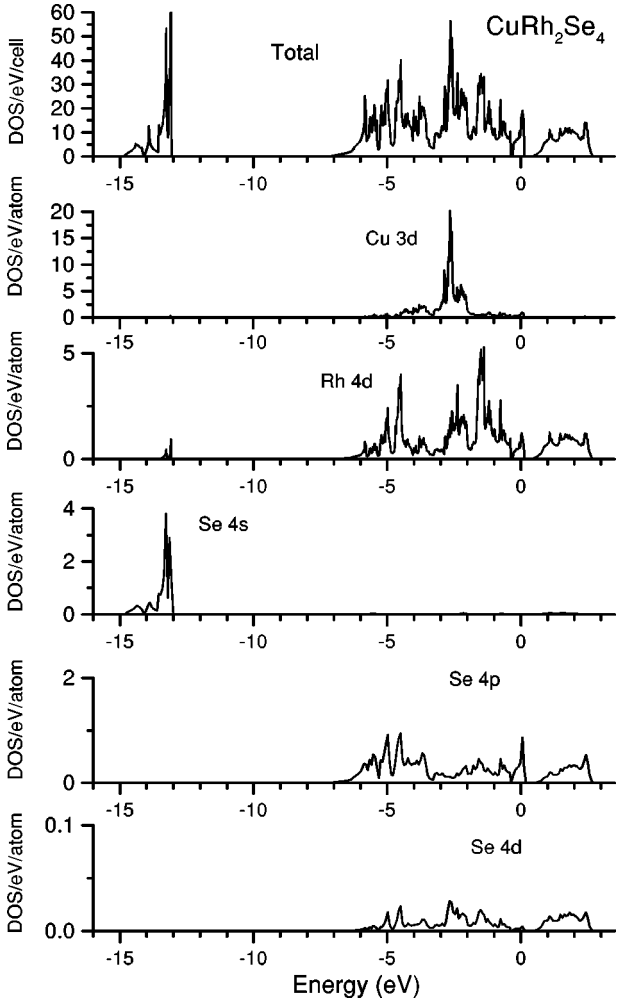

FIG. 8. Calculated total and partial DOS in $CuRh_2Se_4$, as shown for $CuRh_2S_4$ in Fig. 1.

V. OTHER DATA

In a metal the Drude plasma energy tensor $\hbar\Omega_{p,ij}$ contains a good deal of information about low-temperature transport and low-frequency optical properties. $\Omega_{p,ij}$ is given by

$$\Omega_{p,ij}^2 = 4\pi e^2 \frac{1}{V} \sum_k v_{k,i} v_{k,j} \delta(\varepsilon_k - \varepsilon_F) = 4\pi e^2 \langle v_i v_j \rangle N(\varepsilon_F), \tag{1}$$

where $v_{k,i}$ is the ith Cartesian coordinate of the electron velocity, V is the normalization volume, and $\langle \cdots \rangle$ indicates a Fermi surface average. The optical conductivity (specializing now to cubic metals) contains a δ-function contribution at zero frequency proportional to Ω_p^2 (which is broadened by scattering processes), and the static conductivity in Bloch-Boltzmann theory[32] becomes

$$\rho(T) = \rho_0 + \frac{4\pi}{\Omega_p^2 \tau} \tag{2}$$

(ρ_0 is the residual resistivity at $T=0$) as long as the mean free path $l = v_F \tau$ is large enough that scattering processes are independent. When phonon scattering dominates, which is usually the case above 25% of the Debye temperature, the relaxation time τ becomes approximately[33]

$$\frac{\hbar}{\tau_{ep}} = 2\pi \lambda_{tr} k_B T, \tag{3}$$

where λ_{tr} is a ''transport'' electron-phonon (EP) coupling strength that is usually close to the EP coupling constant λ that governs superconducting properties. Then in the high-T regime we obtain the estimate

$$\lambda \approx \lambda_{tr} \approx \frac{\hbar \Omega_p^2}{8\pi^2 k_B} \frac{d\rho}{dT}. \tag{4}$$

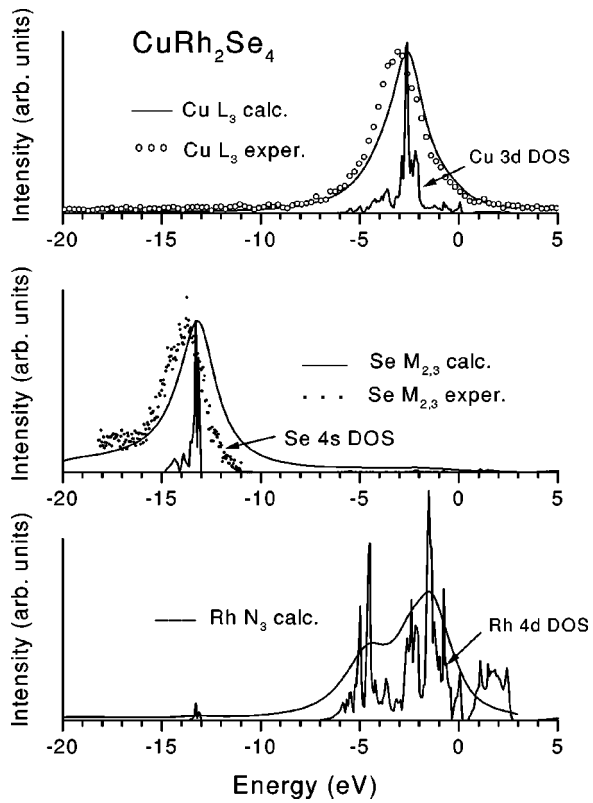

FIG. 9. Comparison of calculated XES and partial DOS with experimental spectra of $CuRh_2Se_4$. The agreement of the main features is within 1 eV (Cu and Se) and even better for Rh.

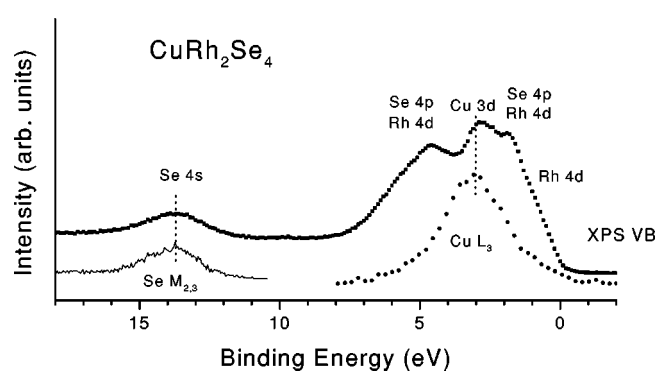

FIG. 10. Comparison of XPS VB to Cu L_3, and Se $M_{2,3}$ XES in $CuRh_2Se_4$. Note the close alignment of the peaks.

Hagino *et al.* (Ref. 4) have presented resistivity data on sintered samples of $CuRh_2S_4$ and $CuRh_2Se_4$. Although both are clearly metallic ($d\rho/dT>0$), the magnitudes of ρ differ by a factor of 20 over most of the range 50 K$\leqslant T\leqslant$300 K. $CuRh_2Se_4$ has $\rho_0=2$ $\mu\Omega$ cm, indicating excellent metallic behavior in spite of the intergrain scattering that is present in the sintered samples. The $CuRh_2S_4$ sample had $\rho_0=500$ $\mu\Omega$ cm (perhaps from intergrain scattering connected to differences in surface chemistry of the sulfide and the selenide) which makes Eq. (2) inapplicable. Moreover, both materials (especially $CuRh_2S_4$) show saturation behavior which makes the Bloch-Boltzmann analysis less definitive. However, we can apply this formalism to $CuRh_2Se_4$ to obtain an estimate, using $d\rho/dT\approx 2\mu\Omega$ cm/K to obtain $\lambda_{tr}=1.8$. This value is almost a factor of 3 larger than $\lambda=0.64$ found by Hagino *et al.* to be sufficient to account for $T_c=3.5$ K. We expect that the magnitude of ρ measured on the sintered sample of $CuRh_2Se_4$, although small, is still not representative of the bulk.

From their measurements, Hagino *et al.*[4] inferred almost indistinguishable values of the linear specific-heat coefficient γ, the density of states $N(E_F)$, and electron-phonon coupling strengths λ for $CuRh_2S_4$ and $CuRh_2Se_4$. (See Table I.) Our calculations lead to a 20% higher value of $N(E_F)$ in the selenide which is at odds with their values. The 1.2 K lower value of T_c in the selenide is not very definitive, since this difference could be related to softer phonon frequencies. The nearly factor of 2 increase in the susceptibility in the selenide (and not in the sulfide) below 300 K remains unexplained. Data on single-crystal samples may be necessary to resolve these discrepancies.

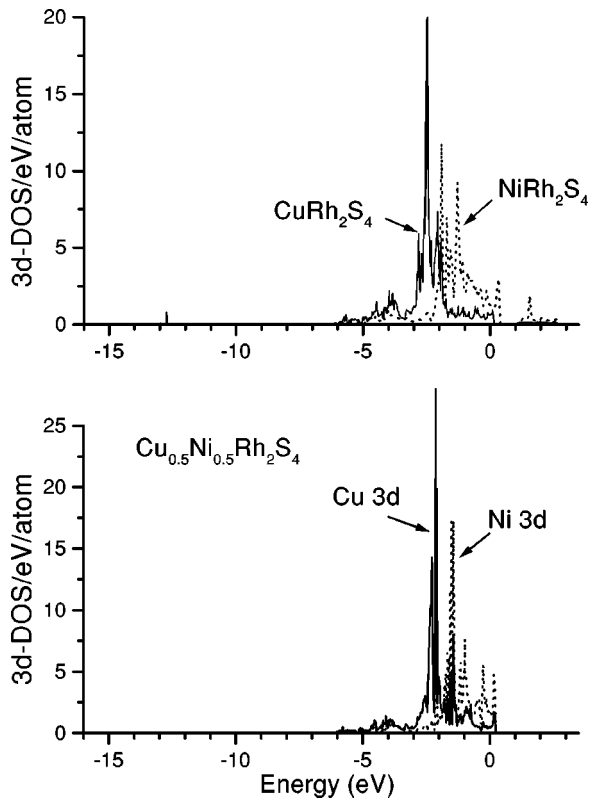

FIG. 11. Comparison of *d* bands from Ni and Cu in $CuRh_2S_4$ and $NiRh_2S_4$ vs $Cu_{0.5}Ni_{0.5}Rh_2S_4$. The significantly different DOS profiles of Ni and Cu *d* states in the pure phases discounts a rigid-band interpretation. In $Cu_{0.5}Ni_{0.5}Rh_2S_4$ we see that the Cu and Ni *d* bands do not mix very strongly, supporting a ''split-band'' interpretation.

VI. CONCLUSIONS

The main results of the present study of the electronic structure in $Cu_{1-x}Ni_xRh_2S_4$ and CuR_2Se_4 can be summarized as follows. The electronic states near E_F consist mainly of Rh $4d$ and S(Se) $3p(4p)$ orbitals for $CuRh_2S_4$ and $CuRh_2Se_4$ and primarily Ni $3d$ with some Rh $4d$ and S $3p$ orbitals in $NiRh_2S_4$. Thus, we find that the character of the states at the Fermi level changes in a non-rigid-band way in $Cu_{1-x}Ni_xRh_2S_4$, and while there is a general trend of a decreasing DOS at the Fermi level as a function of Ni concentration, we have found that the superconducting trends in $Cu_{1-x}Ni_xRh_2S_4$ cannot be explained quantitatively by the calculated DOS of the $Cu_{1-x}Ni_xRh_2S_4$ system. Moreover, such an interpretation would be at odds with the partial DOS which shows the different character of states near E_F. The measured x-ray data suggests interpreting $Cu_{1-x}Ni_xRh_2S_4$ as a solid state solution more in line with a ''split-band'' interpretation. The calculated partial DOS for the 50-50 alloy, see Fig. 11, also suggests this interpretation.

Calculated x-ray emission spectra are found to be in an excellent agreement with experimental data, with peak positions differing by only 0.3–1.0 eV. This agreement implies that core hole effects are negligible. In addition to total DOS, plasma energies have been calculated and used to offer additional theoretical input (see Table I) to interpret the differences between $CuRh_2S_4$ and $CuRh_2Se_4$. Unfortunately, transport data appears to be too strongly affected by intergrain scattering to allow a quantitative analysis.

To summarize, the very good agreement between the measured and calculated electronic spectra indicate a lack of any strong correlation effects. The decrease in superconducting T_c with Ni concentration is likely due to a decrease in $N(E_F)$. Beyond these general conclusions, however, several questions remain. The linear specific heat coefficients are not accounted for quantitatively; neither are the intermediate temperature resistivities, but these must be measured on single crystals to obtain a good experimental picture. Finally, the temperature dependence of the susceptibility of $CuRh_2Se_4$ remains unexplained.

ACKNOWLEDGMENTS

This work was supported by the Russian Science Foundation for Fundamental Research (Project Nos. 96-15-96598 and 98-02-04129), a NATO Linkage Grant (HTECH.LG 971222), INTAS-RFBR (95-0565), NSF Grants (DMR-9017997, DMR-9420425, and DMR-9802076), and the DOE EPSCOR and Louisiana Education Quality Special Fund [DOE-LEQSF (1993-95-03)]. Work at the Advanced Light Source at Lawrence Berkeley National Laboratory was supported by the U.S. Department of Energy under Contract No. DE-AC03-76SF00098. G. L. W. Hart gratefully acknowledges Lawrence Livermore National Laboratory for generously providing computer resources for this work.

*Present address: National Renewable Energy Laboratory, Golden, CO 80401. Electronic address: ghart@nrel.gov

[1] S. Kondo, D. C. Johnston, C. A. Swenson, F. Borsa, A. V. Mahajan, L. L. Miller, T. Gu, A. I. Goldman, M. B. Maple, D. A. Gajewski, E. J. Freeman, N. R. Dilley, R. P. Dickey, J. Merrin, K. Kojima, G. M. Luke, Y. J. Uemura, O. Chmaissem, and J. D. Jorgensen, Phys. Rev. Lett. **78**, 3729 (1997).

[2] D. C. Johnston, J. Low Temp. Phys. **25**, 145 (1976).

[3] S. Nagata, N. Matsumoto, Y. Kato, T. Furubayashi, T. Matsumoto, J. P. Sanchez, and P. Vulliet, Phys. Rev. B **58**, 6844 (1998); E. Z. Kurmaev, V. R. Galakov, D. A. Zatsepin, V. A. Trofimova, S. Stadler, D. L. Ederer, A. Moewes, M. M. Grush, T. A. Callott, J. Matsuno, A. Fujimori, and S. Nagata, Solid State Commun. **108**, 235 (1998); T. Furubayashi, T. Matsumoto, T. Hagino, and S. Nagata, J. Phys. Soc. Jpn. **63**, 3333 (1994); T. Hagino, T. Tojo, T. Atake, and S. Nagata, Philos. Mag. B **71**, 881 (1995).

[4] T. Hagino, Y. Seki, N. Wada, S. Tsuji, T. Shirane, K-I. Kumagai, and S. Nagata, Phys. Rev. B **51**, 12 673 (1995).

[5] J. B. Goodenough, J. Phys. Chem. Solids **30**, 261 (1969).

[6] F. K. Lotgering and R. P. Van Steple, Solid State Commun. **5**, 143 (1967).

[7] N. H. Van Maaren, G. M. Schaeffer, and F. K. Lotgering, Phys. Lett. **25A**, 238 (1967).

[8] M. Robbins, R. C. Willens, and R. C. Miller, Solid State Commun. **5**, 933 (1967).

[9] P. P. Dawes and N. W. Grimes, Solid State Commun. **16**, 139 (1975).

[10] R. N. Shelton, D. C. Johnston, and H. Adrian, Solid State Commun. **20**, 1077 (1976).

[11] G. M. Schaeffer and M. H. Van Maaren, in *Proceedings of the 11th International Conference on Low Temperature Physics*, edited by J. F. Allen (University of St. Andrews Press, St. Andrews, Scotland, 1969), Vol. 2, p. 1033.

[12] M. H. Van Maaren, H. B. Harland, and I. E. Havinga, Solid State Commun. **8**, 1933 (1970).

[13] T. Bitoh, T. Hagino, Y. Seki, S. Chikazawa, and S. Nagate, J. Phys. Soc. Jpn. **61**, 3011 (1992).

[14] T. Shirane, T. Hagino, Y. Seki, T. Bitoh, S. Chikazawa, and S. Nagata, J. Phys. Soc. Jpn. **62**, 374 (1993).

[15] Z. W. Lu, B. M. Klein, E. Z. Kurmaev, V. M. Cherkashenko, V. R. Galakhov, S. N. Shamin, Yu. M. Yarmoshenko, V. A. Trofimova, St. Uhlenbrock, M. Neumann, T. Furubayashi, T. Hagino, and S. Nagata, Phys. Rev. B **53**, 9626 (1996).

[16] J. Matsuno, T. Mizokawa, A. Fujimori, D. A. Zatsepin, V. R. Galakhov, E. Z. Kurmaev, Y. Kato, and S. Nagata, Phys. Rev. B **55**, R15 979 (1997).

[17] A. V. Postnikov *et al.* (unpublished).

[18] N. Matsumoto, H. Honma, Y. Kato, S. Yasuzuka, K. Morie, N. Kijima, S. Ebisu, and S. Nagata, *Advances in Superconductivity IX: Proceedings of the 9th International Symposium on Superconductivity* (Springer-Verlag, Tokyo, 1997), p. 175.

[19] T. Oda, M. Shirai, N. Suzuki, and K. Motizuki, J. Phys.: Condens. Matter **7**, 4433 (1995).

[20] J. J. Jia, T. A. Callcott, J. Yurkas, A. W. Ellis, F. J. Himpsel, M. G. Samant, J. Stöhr, D. L. Ederer, and R. C. C. Perera, Rev. Sci. Instrum. **66**, 1394 (1995).

[21] P. Blaha, K. Schwarz, and J. Luitz, WIEN97, Vienna University of Technology, Vienna, 1997; updated version of P. Blaha, K. Schwarz, P. Sorantin, and S. B. Trickey, Comput. Phys. Commun. **59**, 399 (1990).

[22] J. P. Perdew and Y. Wang, Phys. Rev. B **45**, 13 244 (1992).

[23] J. P. Perdew, S. Burke, and M. Ernzerhof, Phys. Rev. Lett. **77**, 3865 (1996).

[24] P. E. Blöchl, O. Jepsen, and O. K. Andersen, Phys. Rev. B **49**, 16 223 (1994).

[25] A. Neckel, K. Schwarz, R. Eibler, and P. Rastl, Microchim. Acta, Suppl. **6**, 257 (1975).

[26] There are several differences between our calculations and those of Ref. 19. The most significant difference is that many fewer basis functions ($\sim$50/atom) were used in the previous calculations (we used $\sim$100 basis functions/atom) and the exchange-correlation potentials were also different.

[27] S. Nagata (unpublished).

[28] Rh N_3 XES spectra were not measured.

[29] Split band behavior is also found in CuNi. See G. M. Stocks, R. W. Williams, and J. S. Faulkner, Phys. Rev. Lett. **26**, 253 (1971).

[30] Cu L_3 and Ni L_3 XES are converted to binding energies using our XPS measurements of corresponding core levels.

[31] J. J. Yeh and I. Lindau, At. Data Nucl. Data Tables **32**, 1 (1985).

[32] J. M. Ziman, *Electrons and Phonons* (Clarendon Press, Oxford, 1962), Chap. VII and IX.

[33] P. B. Allen, Phys. Rev. B **13**, 1416 (1976); **17**, 3725 (1978).